*J. PharmTechNova.* Volume: 01; Issue: 03; Year: 26; Pages: 126-151
DOI: https://doi.org/10.66220/qap0cz96

A.S. Ghadage et al.
ISSN: 3139-9258

**Journal of PharmTechNova (JPTN)**
**https://pharmtechnova.com/index.php/jptn**

*Research Article*

# Development and Optimization of a Luliconazole Film-Forming Topical Spray Using a Quality by Design Approach

**Avanti S. Ghadage[1], Madan D. Pomaje[1], Ashwini B. Patil[2]**

[1]Department of Pharmaceutics, Govindrao Nikam College of Pharmacy, Sawarde, Ratnagiri, Maharashtra, India.
[2]Department of Pharmaceutical Chemistry, Govindrao Nikam College of Pharmacy, Sawarde, Ratnagiri, Maharashtra, India.

*Corresponding author/author's: awantighadage14@gmail.com

**Article info:**
**Submitted:** 27/09/2026
**Revised:** 17/10/2026
**Accepted:** 18/10/2026
**Published:** 21/10/2026
**Manuscript ID:** 00031
**Subject:** Pharmaceutical Technology and Drug Development

**Keywords:**
Luliconazole; Film-forming spray; Topical drug delivery; Quality by Design; Factorialdesign; Formulation optimization.

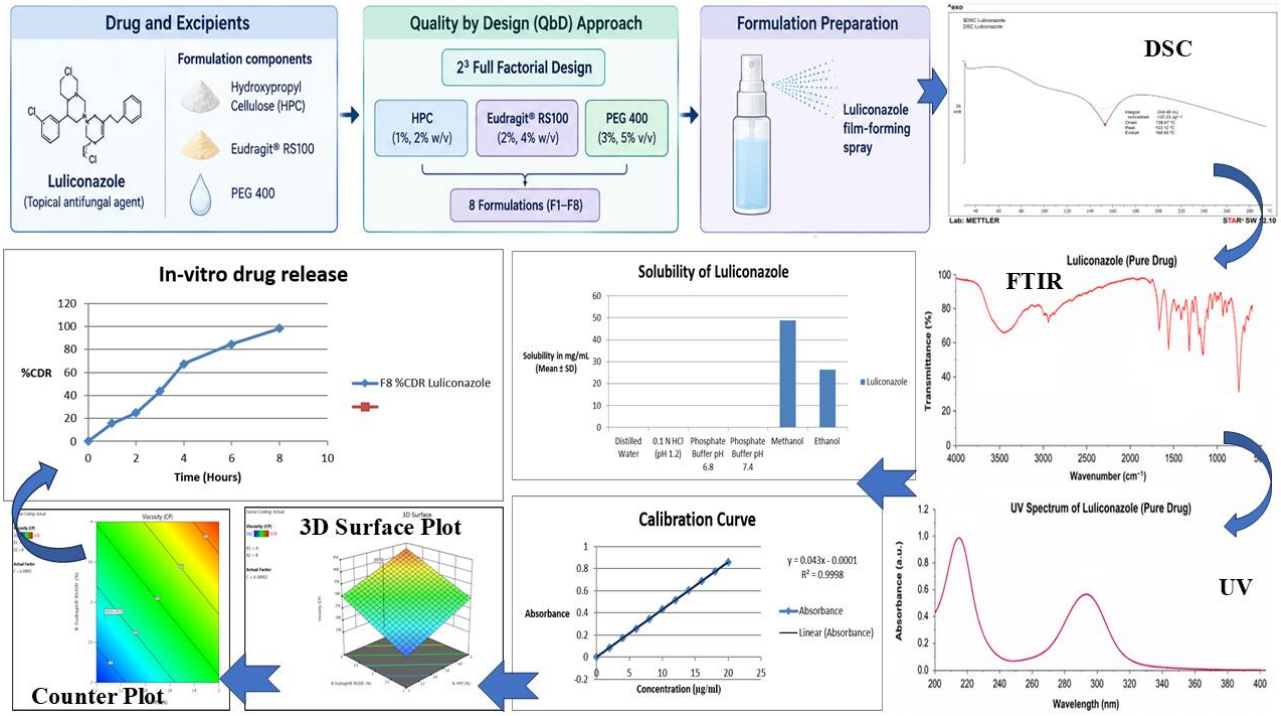
**Abstract:**
Luliconazole is a topical antifungal agent used in the management of superficial fungal infections. Film-forming topical sprays may provide convenient application and facilitate the formation of a uniform drug-containing film at the site of administration. The present study aimed to develop and optimize a Luliconazole film-forming spray using a Quality by Design (QbD) approach. A (2^3) full factorial design was employed to investigate the effects of Hydroxypropyl Cellulose (HPC), Eudragit® RS100, and PEG 400 on critical formulation responses, with drying time and viscosity selected as dependent variables. Eight formulations (F1–F8) were prepared by varying the concentrations of the selected formulation components and evaluated for appearance, film formation, pH, viscosity, drying time, spray angle, film thickness, folding endurance, stickiness, washability, leak test, drug content, and in vitro drug diffusion. Statistical analysis and response-surface methodology were used for formulation optimization. The prepared formulations were clear and homogeneous and exhibited acceptable film-forming properties. Drying time ranged from 3.8 to 8.2 min, while viscosity ranged from 162 to 438 cP. The formulation variables significantly influenced the investigated responses. Formulation F8, containing 1% w/v HPC, 4% w/v Eudragit® RS100, and 5% v/v PEG 400, was selected as the optimized formulation. F8 exhibited a drying time of 5.1 min, viscosity of 304 cP, and spray angle of 83.6°. It produced a uniform, transparent, non-sticky, and adherent film, with drug content of 99.2 ± 0.8%. The QbD approach enabled systematic optimization of the Luliconazole film-forming spray and identified F8 as a promising formulation with desirable spray and film-forming characteristics for topical drug delivery.

**How to Cite this article:** A.S. Ghadage, M.D. Pomaje, A.B. Patil. Development and Optimization of a Luliconazole Film-Forming Topical Spray Using a Quality by Design Approach. *J. PharmTechNova.* **2026**, 01 [03], 126-151. DOI: https://doi.org/10.66220/qap0cz96

**©2026 The authors**
**This is an Open Access article distributed under the terms of the Creative Commons Attribution (CC BY NC), which permits unrestricted use, distribution, and reproduction in any medium, as long as the original authors and source are cited. No permission is required from the authors or the publishers. (https://creativecommons.org/licenses/by-nc/4.0/)**

DOI: https://doi.org/10.66220/qap0cz96 ISSN: 3139-9258

## Graphical Abstract




## 1. Introduction

Superficial fungal infections represent a substantial global health burden, particularly in tropical and subtropical regions, where warm and humid environmental conditions favor the growth and transmission of pathogenic fungi. Dermatophytosis and other superficial mycoses commonly affect the skin and may result in erythema, pruritus, scaling, inflammation, and discomfort, thereby adversely affecting patients' quality of life. Conventional topical antifungal dosage forms, including creams, ointments, and gels, are widely employed for the management of localized fungal infections. However, these formulations may exhibit limitations, such as poor patient acceptability, greasiness, inadequate residence time, repeated application requirements, and removal by clothing, sweating, or washing. Consequently, the development of innovative topical delivery systems capable of improving drug deposition, convenience, and patient compliance has gained considerable attention.

Luliconazole is a synthetic imidazole antifungal agent with potent activity against a broad spectrum of dermatophytes. It exerts its antifungal effect primarily by inhibiting lanosterol 14$\alpha$-demethylase, an enzyme involved in ergosterol biosynthesis, thereby disrupting fungal cell membrane integrity. Although luliconazole demonstrates favorable antifungal potency, effective topical therapy depends not only on the pharmacological activity of the drug but also on the characteristics of the formulation and its ability to deliver and maintain the drug at the site of infection. Therefore, formulation strategies that facilitate uniform application, rapid film formation, prolonged residence, and efficient drug release may offer advantages over conventional semisolid preparations.

Film-forming topical sprays have emerged as promising drug-delivery systems for localized dermatological therapy. Following application, the volatile components of the formulation evaporate, leaving behind a thin, uniform polymeric film containing the active pharmaceutical ingredient. Such systems can provide improved coverage of the affected skin, reduce direct contact during application, and potentially enhance formulation residence at the administration site. The spray format may also facilitate convenient application over irregular, extensive, or difficult-to-reach skin surfaces. However, development of a film-forming spray requires careful optimization of multiple formulation and process variables, including polymer

DOI: https://doi.org/10.66220/qap0cz96 ISSN: 3139-9258

concentration, solvent composition, plasticizer level, spray characteristics, drying behavior, viscosity, drug content, film integrity, and drug-release properties. Changes in one variable may influence several critical quality attributes simultaneously, making systematic formulation development essential.

Quality by Design (QbD) provides a science- and risk-based framework for the systematic development and optimization of pharmaceutical formulations. The approach begins with defining the quality target product profile (QTPP), identifying critical quality attributes (CQAs), determining critical material attributes (CMAs) and critical process parameters (CPPs), and evaluating their potential effects through risk assessment and experimental studies. Design of Experiments (DoE) can subsequently be employed to establish relationships between formulation variables and CQAs while reducing the number of experimental trials and facilitating the identification of an optimized formulation. Such an approach can improve product understanding, reproducibility, and robustness compared with conventional trial-and-error formulation development.

In this context, the present study focuses on the development and optimization of a luliconazole film-forming topical spray using a Quality by Design approach. The formulation development strategy involves systematic identification and evaluation of critical formulation variables, followed by optimization based on predefined quality attributes. The optimized formulation is intended to provide desirable sprayability, rapid film formation, satisfactory physical characteristics, uniform drug distribution, and appropriate drug-release behavior. The application of QbD principles is expected to provide a rational and scientifically justified basis for developing a robust luliconazole topical spray with potential advantages in convenience, patient acceptability, and effective localized antifungal therapy.

## 2. Materials and Methods

### 2.1. Drug Purchase and Procurement

Pure Luliconazole with analytical grade was purchased from a laboratory trading laboratory in Chhatrapati Sambhajinagar. The obtained drug samples were subjected to formal preliminary investigation to identify the samples.

### 2.2. Determination of Melting Points

The melting point of the pharmaceutical compound was ascertained using a digital capillary melting point device employing the capillary technique. Prior to analysis, the sample was finely powdered using a clean, dry mortar and pestle to ensure uniform particle size. If required, the sample was dried to remove residual moisture. A minimal amount of the powdered substance was inserted into a slender glass capillary tube that was sealed at one extremity. The capillary was gently tapped on a hard surface to compact the sample, ensuring a uniform column of approximately 2–3 mm in height without air gaps (1,2).

The filled capillary tube was placed in the sample holder of the melting point apparatus, ensuring alignment with the temperature sensor. The apparatus was switched on and initially heated rapidly to approximately 10°C below the expected melting temperature of the drug (as per literature value). Thereafter, the heating rate was reduced to 1–2°C per minute to obtain an accurate measurement. The sample was observed through the magnifying lens of the apparatus, and the temperatures corresponding to the onset of melting (first visible sign of liquefaction) and completion of melting (formation of a clear liquid) were recorded. The melting point was expressed as the temperature range between the onset and clear point. All determinations were performed in triplicate, and the mean melting point range was reported. The apparatus was calibrated prior to analysis to ensure the accuracy of the temperature measurement.

### 2.3. DSC Analysis

DSC analysis was performed to evaluate the thermal behavior and melting characteristics of the drug substance using a Mettler Toledo DSC instrument (STARe SW software version 12.10) (3–7). The device was adjusted for temperature and enthalpy using established reference substances (e.g., indium) before the analysis.

DOI: https://doi.org/10.66220/qap0cz96 ISSN: 3139-9258

Approximately 3–5 mg of accurately weighed sample was placed in a standard aluminum DSC pan and hermetically sealed. An empty sealed aluminum pan of the same type was used as the reference. The sample pan and reference pan were positioned in the DSC cell, and the analysis was carried out under a continuous purge of dry nitrogen gas to maintain an inert atmosphere and prevent oxidative degradation.

The sample was heated over a temperature range of 30–300°C at a controlled heating rate of 10°C/min. The heat flow was recorded as a function of temperature, and thermograms were obtained in the exothermic-up mode. The onset temperature (T_onset), peak temperature (T_peak), and endset temperature (T_endset) of the melting transition were determined directly from the thermogram using the instrument software by applying baseline correction and peak integration. The enthalpy of fusion (ΔH_fus) was calculated from the area under the endothermic peak and expressed in J/g after normalization with respect to the sample weight. The thermograms were analyzed to assess the crystalline nature, purity, and possible polymorphic transitions of the drug substance.

**2.4. FTIR Spectroscopic Analysis**

FTIR spectroscopy was performed to characterize the functional groups and assess the chemical integrity of the drug substance (8–10). The examination was conducted using an FTIR spectrophotometer fitted with a direct sample holder/ATR (Attenuated Total Reflectance) attachment. A small quantity of the sample was placed directly onto the sample holder without any prior potassium bromide (KBr) pellet preparation. The sample was gently pressed to ensure adequate contact with the crystal surface to obtain optimal spectral resolution.

The spectra were recorded over a wavenumber range of 4000–400 $cm^{-1}$ at ambient temperature. Each spectrum was acquired by accumulating 16–32 scans at a resolution of 4 $cm^{-1}$ to improve the signal-to-noise ratio. A background spectrum was recorded prior to sample analysis and automatically subtracted from the sample spectrum to eliminate atmospheric interference. The obtained spectra were analyzed using the instrument's software to identify characteristic absorption bands corresponding to specific functional groups present in the drug molecule. The observed peaks were compared with reported literature values to confirm structural integrity and to detect any potential chemical interactions or degradation. All measurements were performed under identical instrumental conditions to ensure reproducibility of the results.

**2.5. Solubility Determination (Shake Flask Method)**

The solubility of luliconazole was assessed using the equilibrium shake-flask method, which is the conventional approach for saturation solubility investigations (11,12).
An abundant quantity of the medication was incorporated into 10 mL of the chosen solvent inside securely sealed glass vials to guarantee saturation. The vials were secured and positioned on a temperature-regulated orbital shaker set at 25 ± 0.5°C (or 37 ± 0.5°C, contingent upon the research design) and stirred at 100 rpm for 24–48 h to reach equilibrium. Upon equilibration, the samples were visually examined to verify the existence of undissolved medication, signifying saturation. The suspensions were then subjected to centrifugation at 5000 rpm for 15 min and passed through a 0.45-μm membrane filter to exclude undissolved particles.

A portion of the transparent filtrate was appropriately diluted with the relevant solvent and examined spectrophotometrically using a UV–visible spectrophotometer at the specified λmax for each pharmaceutical compound. The amount of dissolved medication was determined using a calibration curve that was previously established. All experiments were conducted in triplicate, and the results are reported as mean ± standard deviation (mg/mL).

**2.6. UV–Visible Spectrophotometric Analysis and Calibration Curve Construction**

UV–visible spectrophotometry was employed to determine the maximum absorbance wavelength (λmax) of luliconazole and to establish a calibration curve for its quantitative estimation. The calibration curve

DOI: https://doi.org/10.66220/qap0cz96 ISSN: 3139-9258

was generated by measuring the absorbance of standard luliconazole solutions at the selected λmax, providing a reliable method for subsequent quantitative analysis (13–15).

#### *2.6.1 Determination of λmax*

A primary stock solution of luliconazole (1000 µg/mL) was prepared by accurately weighing 10 mg of the drug and dissolving it in methanol in a 10 mL volumetric flask. The stock solution was further diluted with the same solvent to obtain working solutions in the concentration range of 10–20 µg/mL.

The prepared solution was scanned using a UV–Visible spectrophotometer within the wavelength range of 200–400 nm, with methanol serving as the blank. The wavelength exhibiting the highest absorbance was identified and recorded as the λmax of luliconazole from the obtained absorption spectrum.

### 2.7 Preparation of Calibration Curve

#### *2.7.1 Preparation of Standard Solutions*

A secondary stock solution (100 µg/mL) was prepared by appropriately diluting the primary stock solution (1000 µg/mL) with methanol. From this solution, a series of working standard solutions covering the required linearity range (e.g., 2–20 µg/mL) was prepared through serial dilution.

#### *2.7.2 Measurement of Absorbance*

The absorbance of each standard solution was recorded at the predetermined λmax using a UV–Vis spectrophotometer, with methanol employed as the blank (16,17). Each measurement was carried out in triplicate to ensure precision and reproducibility of the analytical results.

#### *2.7.3 Construction of Calibration Curve*

The calibration curve was established by plotting the concentrations of the standard solutions (µg/mL) against their corresponding absorbance values (18,19). Linear regression analysis was performed to determine the calibration equation, which was subsequently used for the quantitative estimation of luliconazole.

$$A = mC + b \quad -----(1)$$

where:
**A** = Absorbance
**C** = Concentration (µg/mL)
**m** = Slope
**b** = Intercept

The correlation coefficient ($R^2$) was calculated to evaluate linearity. The method was considered linear within the selected concentration range if $R^2 \geq 0.99$.

### 2.8 Determination of Drug–Excipient Compatibility

Drug–excipient compatibility studies were performed to evaluate the potential physicochemical interactions between the active pharmaceutical ingredients (APIs) and selected excipients using FTIR spectroscopy and DSC. This study was conducted as part of the preformulation investigations to ensure formulation stability and integrity (3–7).

Accurately weighed quantities of drug and excipient were mixed in a 1:1 ratio (w/w) unless otherwise specified. The components were gently triturated in a mortar and pestle to ensure uniform blending. The prepared mixtures were stored in airtight glass containers and protected from light and moisture until further analysis. The prepared mixtures were subjected to FTIR and DSC analyses to determine their chemical and physical stabilities.

DOI: https://doi.org/10.66220/qap0cz96 ISSN: 3139-9258

### 2.9 Formulation of combined spray formulation dosage form by QBD approach

#### *2.9.1 Statistical DOE*

A $2^3$ full factorial design was employed for the preparation and optimization of a topical film-forming antifungal and steroidal spray containing luliconazole. The concentrations of hydroxypropyl cellulose (HPC) (A, % w/v), Eudragit® RS100 (B, % w/v), and PEG 400 (C, % v/v) were selected as independent variables and evaluated at two levels (-1 and +1). The influence of the selected formulation variables on the drying time ($Y_1$) and viscosity of the resulting film ($Y_2$) were evaluated as the response variables. The independent variables and their respective levels are summarized in Table 1. The experimental data generated from the design were statistically analyzed using Design-Expert® software to assess the effects of the formulation variables and optimize the formulation.

**Table 1.** Variables and levels

| Variable | (-1) Low level | (+1) High level |
|---|---|---|
| **Independent** | | |
| **A= Hydroxypropyl Cellulose (HPC)** | 1% | 2% |
| **B= Eudragit® RS100** | 2% | 4% |
| **C= PEG 400** | 5% | 10% |
| **Dependent** | | |
| **Y1= Drying time** | | |
| **Y2 = Viscosity** | | |

#### *2.9.2 Preparation of Luliconazole Film-Forming Spray*

Luliconazole film-forming spray formulations were prepared according to a $2^3$ full factorial design using Hydroxypropyl Cellulose (HPC, 1–2% w/v), Eudragit® RS100 (2–4% w/v), and PEG 400 (5–10% v/v) as independent variables. HPC and Eudragit® RS100 were dissolved in ethanol under continuous stirring to obtain a clear polymeric solution. Luliconazole was first dissolved in PEG 400 and then gradually incorporated into the polymeric solution under continuous stirring to ensure uniform dispersion. The volume of the formulation was adjusted to 100 mL with ethanol, followed by further stirring until a clear, homogeneous, and stable film-forming spray solution was obtained. Eight formulations (F1–F8) were prepared according to the experimental design matrix.

### 2.10 Evaluation of Spray Formulation

#### *2.10.1 Appearance and Film Formation*

The prepared Luliconazole film-forming spray formulations were evaluated visually for their appearance, including clarity, color, homogeneity, and film-forming ability. The formulations were sprayed onto a clean glass slide and observed for the formation of a uniform, transparent, non-sticky film with good adhesion to the surface.

#### *2.10.2 Viscosity*

The viscosity of the developed film-forming spray formulations was measured using a Brookfield viscometer (Model LV-DV-II, Brookfield Engineering Laboratories, USA) fitted with a suitable spindle (20,21). All measurements were performed at ambient temperature (25 ± 2°C), and the viscosity was expressed in centipoise (cP).

#### *2.10.3 pH*

The pH of each formulation was determined using a calibrated digital pH meter. Before measurement, the instrument was calibrated using standard buffer solutions of pH 4.0, 7.0, and 9.0. The pH readings were

DOI: https://doi.org/10.66220/qap0cz96 ISSN: 3139-9258

recorded at room temperature, and the mean value of three independent measurements was calculated and reported.

#### *2.10.4 Evaporation time*

The drying time of the film-forming spray was determined by spraying a fixed quantity of the formulation onto a clean glass surface. The time required for the sprayed solution to form a completely dry, uniform film was recorded using a stopwatch. All examinations were conducted at ambient temperature (25±2°C), and the mean value of three assessments was recorded. This parameter was used to assess the film-forming efficiency and patient convenience of the formulation.

#### *2.10.5 Spray angle*

The spray angle was determined by actuating the formulation horizontally onto a white sheet of paper positioned 10 cm from the spray nozzle. The diameter of the resulting spray pattern was measured, and the radius (r) was calculated. The spray angle (θ) was then determined using the following equation:

$$\text{Spray angle } (\theta) = \tan^{-1} (l/r) \quad \ldots\ldots\ldots\ldots\ldots\ldots \quad (2)$$

where l represents the distance between the nozzle and the paper (10 cm), and **r** denotes the radius of the circular spray pattern.

### 2.11 Evaluation of Film

#### *2.11.1 Thickness of the films*

The thickness of the dried film was determined using a screw gauge by measuring at different locations on the film surface. The average of the recorded measurements was calculated and expressed as the film thickness.

#### *2.11.2 Film Flexibility*

Film flexibility was evaluated by determining the folding endurance. A film strip (approximately 2 × 2 cm) was repeatedly folded at the same point until it showed signs of breaking. The total number of folds the film withstood before breaking was recorded as the folding endurance.

#### *2.11.3 Stickiness of the film*

The surface stickiness of the dried film was assessed by gently pressing cotton wool onto the film under light pressure. The extent of cotton fiber adherence was visually examined and graded as high (dense fiber attachment), medium (partial fiber adherence), or low (minimal or no fiber attachment).

#### *2.11.4 Washability and leak test*

The film was placed under a controlled flow of simulated fluid (e.g., simulated saliva, pH 6.8, or phosphate buffer, pH 7.4) to observe the dissolution or erosion time. The film was attached to a water-resistant backing and placed against a moist surface or filled with fluid to monitor for any outward leakage of the drug formulation.

#### *2.11.5 Drug content*

Drug content was determined by cutting a film sample (5 × 5 mm) from different regions of the prepared film. Each sample was transferred to a 100 mL volumetric flask containing 100 mL of distilled water and allowed to dissolve completely. The resulting solution was analyzed using a UV–Visible spectrophotometer at 296 nm to determine the drug content.

DOI: https://doi.org/10.66220/qap0cz96 ISSN: 3139-9258

#### *2.11.6 In-vitro diffusion study using eggshell membrane (In-vitro drug release)*

An *in vitro* drug diffusion study of the luliconazole film-forming spray was performed using a Franz diffusion cell with an eggshell membrane as the diffusion barrier. Prior to the experiment, the eggshell membrane was hydrated by soaking it in phosphate buffer (pH 7.4) for 24 h. The hydrated membrane was then mounted between the donor and receptor compartments of the diffusion cell.

The receptor compartment was filled with phosphate buffer (pH 7.4) containing 20% (v/v) methanol, which served as the diffusion medium. The medium was maintained at 37 ± 0.5°C and continuously stirred at 50 rpm using a magnetic stirrer throughout the experiment. An accurately measured volume (0.5 mL) of the formulation was placed in the donor compartment over the membrane.

At predetermined time intervals, 1 mL aliquots were withdrawn from the receptor compartment and immediately replaced with an equal volume of fresh preheated diffusion medium to maintain constant volume and sink conditions. The collected samples were analyzed by UV–Visible spectrophotometry at 296 nm, and the cumulative percentage of drug diffusion was calculated.

### 2.12 Kinetics of drug release

#### *2.12.1 Zero order*

The zero-order kinetic model is commonly applied to controlled and sustained drug delivery systems, including transdermal patches, coated dosage forms, and matrix-based formulations containing poorly water-soluble drugs (22–24). In this model, the drug is released at a constant rate, independent of its concentration. The equation describing zero-order drug release is

$$Qt = Q_0 + K_0t \text{ --------- (2)}$$

Where:

- Qt = Amount of drug released at time *t*
- $Q_0$ = Initial amount of drug in the formulation
- $K_0$ = Zero-order release rate constant

#### *2.12.2 First order*

The first-order kinetic model describes drug release systems in which the release rate depends on the amount of drug remaining in the dosage form. Consequently, the drug release decreases progressively over time as the concentration diminishes (22–24). The model is represented by the following equation:

$$\log Qt = \log Q_0 + (K_1t / 2.303) \text{ --------- (3)}$$

Where:

- Qt = Amount of drug released at time *t*
- $Q_0$ = Initial amount of drug present
- $K_1$ = First-order release rate constant

#### *2.12.3 Higuchi Model*

The Higuchi model is widely used to describe drug release from solid and semisolid matrix systems, particularly where diffusion is the primary release mechanism (22–24). The mathematical expression is given as

$$Q = [D (2C - Cs) Cs t]^{1/2} \text{ --------- (4)}$$

DOI: https://doi.org/10.66220/qap0cz96 ISSN: 3139-9258

Where:

- Q = Cumulative amount of drug released per unit area at time *t*
- C = Initial drug concentration
- Cs = Drug solubility in the matrix
- D = Diffusion coefficient

Assuming that the diffusion coefficient and other formulation parameters remain constant during drug release, the equation simplifies to:

$$Q = K\sqrt{t}$$

A linear relationship between cumulative drug release and the square root of time indicates diffusion-controlled release. The suitability of this model was assessed using linear regression analysis and the corresponding regression coefficient ($R^2$).

#### *2.12.4 Korsmeyer Peppas*

The Korsmeyer–Peppas model was employed to investigate the mechanism of drug release from the developed formulations (22–24). The model relates the fraction of drug released to time using the following equation:

$$Q = Kt^n$$

Taking the logarithm of both sides gives:

$$\log Q = \log K + n \log t \text{ --------- (5)}$$

Where:

- Q = Cumulative percentage of drug released
- K = Release rate constant
- t = Time
- n = Release exponent, indicating the mechanism of drug release

The values of n obtained from the slope of the log Q versus log t plot were used to characterize the drug release mechanism.

### 2.13 Accelerated stability studies

The optimized luliconazole film-forming spray formulation was subjected to accelerated stability testing for three months, following the ICH guidelines (25,26). The formulation was stored in tightly sealed containers under controlled conditions of 30 ± 2°C and 75 ± 5% relative humidity (RH). Samples were analyzed at the beginning of the study (0 month) and after three months of storage for physical appearance, pH, and viscosity to evaluate the stability of the formulation during the storage period.

## 3. Results and Discussion

### 3.1 Determination of Melting Points

The melting point of luliconazole was determined to be 149–154°C. The observed melting range was in close agreement with the reported literature values, confirming the identity and purity of the drug. The narrow melting range indicates the absence of significant impurities and reflects the crystalline nature of luliconazole.

DOI: https://doi.org/10.66220/qap0cz96 ISSN: 3139-9258

These findings suggest that the drug possesses adequate thermal stability and is suitable for further preformulation and formulation studies.

**3.2 DSC analysis**

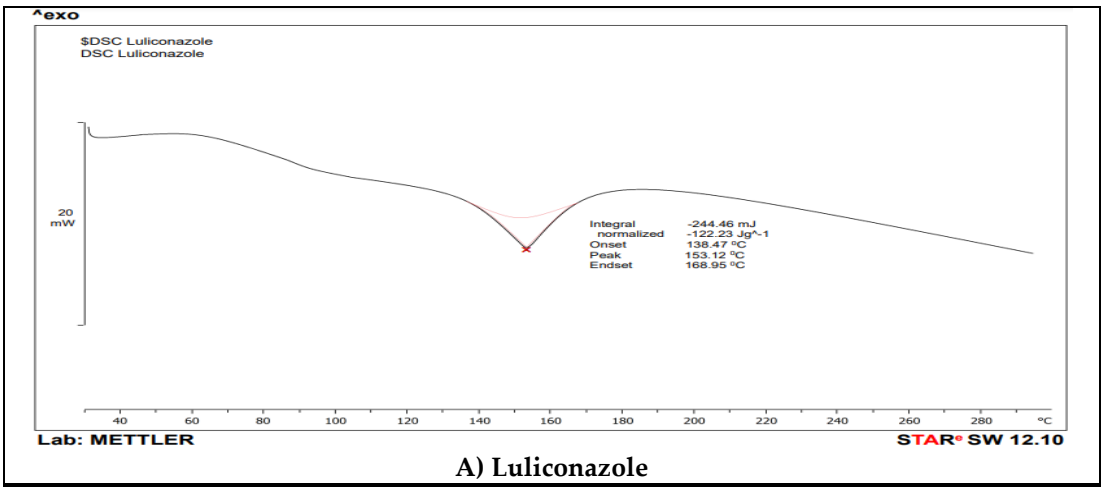
DSC was performed to evaluate the thermal behavior of Luliconazole, individual excipients, and their physical mixture to investigate possible drug–excipient interactions and assess the compatibility of formulation components (Figure 1). The DSC thermogram of pure Luliconazole exhibited a sharp and distinct endothermic melting peak at 153.12°C (onset: 138.47°C; endset: 168.95°C) with a heat of fusion (ΔH = −122.23 J/g), confirming the crystalline nature and characteristic melting behavior of the drug.

The selected excipients exhibited their respective thermal transitions. HPMC showed a broad endothermic peak at 72.98°C (ΔH = −99.31 J/g), which can be attributed primarily to the evaporation of absorbed moisture owing to the hygroscopic nature of the polymer. PEG 400 exhibited an endothermic transition at 79.18°C (ΔH = −133.63 J/g), corresponding to its thermal response during heating. Eudragit RS-100 displayed a broad thermal transition at 140.87°C (ΔH = −109.44 J/g), associated with polymer softening and thermal degradation-related changes. Similarly, hydroxypropyl cellulose exhibited a broad endothermic event at 214.27°C (ΔH = −155.34 J/g), which may be related to polymer chain relaxation and thermal decomposition.

The DSC thermogram of the physical mixture showed multiple endothermic transitions corresponding to the combined thermal behavior of the drug and excipients, with characteristic peaks observed at 68.81°C, 129.91°C, 162.41°C, and 220.19°C. The characteristic melting endotherm of luliconazole was retained and observed at 162.41°C (onset: 153.46°C; endset: 188.59°C; ΔH = −177.13 J/g). The slight elevation in the melting temperature compared with pure luliconazole may be attributed to the presence of polymeric excipients, physical mixing effects, and altered heat transfer during analysis. However, the preservation of the characteristic drug melting peak indicates that the crystalline structure of luliconazole remained intact within the physical mixture.

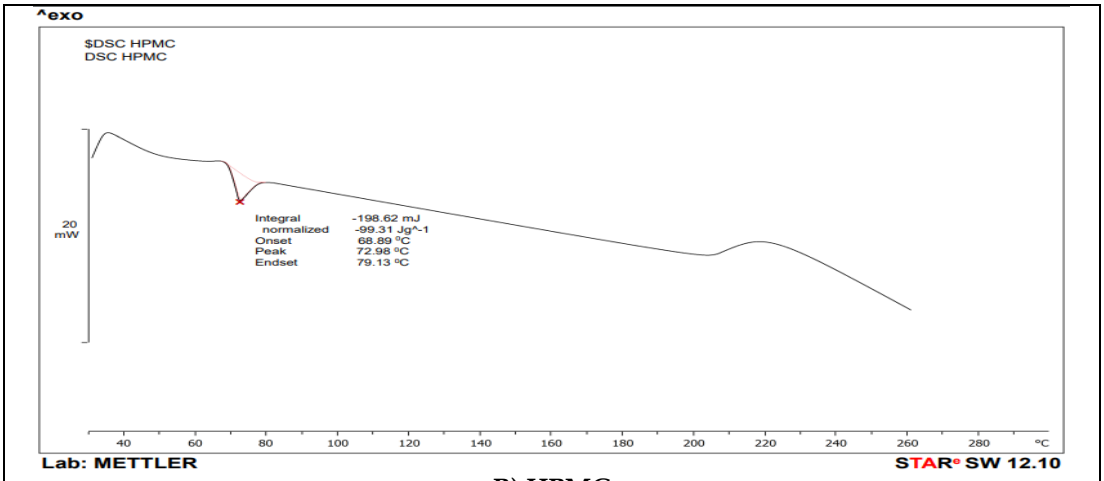
Furthermore, the absence of new endothermic or exothermic events and the retention of characteristic thermal transitions of both the drug and excipients suggest that no significant chemical interaction or solid-state transformation occurred during mixing. The observed variations in peak position and enthalpy values may be associated with dilution effects, changes in molecular mobility, and weak intermolecular interactions, such as hydrogen bonding between luliconazole and formulation components. Importantly, the absence of peak disappearance, major melting point depression, or formation of additional thermal events rules out the possibility of incompatibility, eutectic formation, or degradation.

Overall, DSC analysis confirmed the physical compatibility of luliconazole with HPMC, PEG 400, Eudragit RS-100, and hydroxypropyl cellulose, indicating that the selected excipients are suitable for further formulation development without inducing undesirable solid-state changes in the drug.

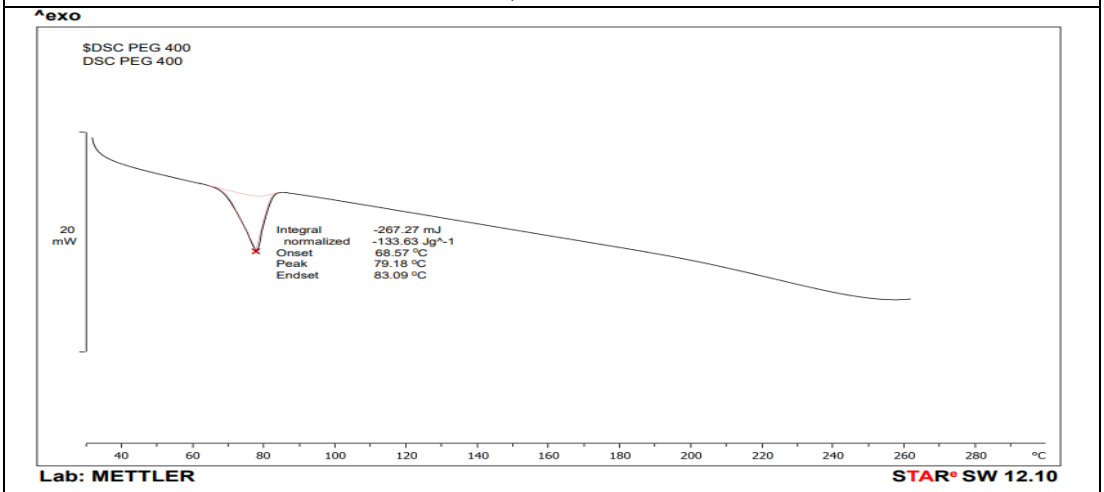



**A) Luliconazole**

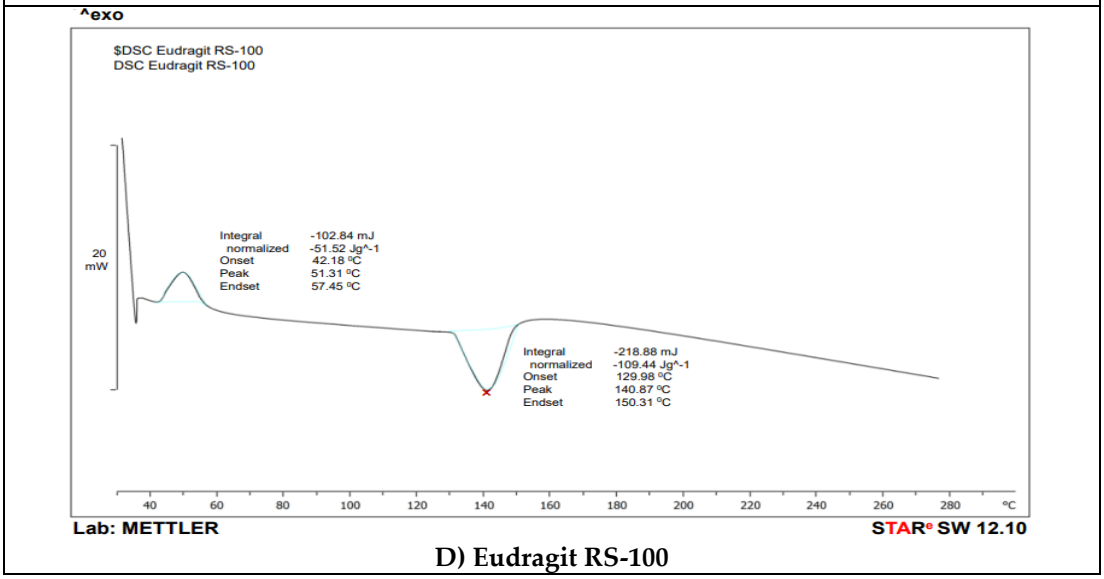
DOI: https://doi.org/10.66220/qap0cz96 ISSN: 3139-9258




**B) HPMC**




**C) PEG 400**




**D) Eudragit RS-100**

DOI: https://doi.org/10.66220/qap0cz96 ISSN: 3139-9258

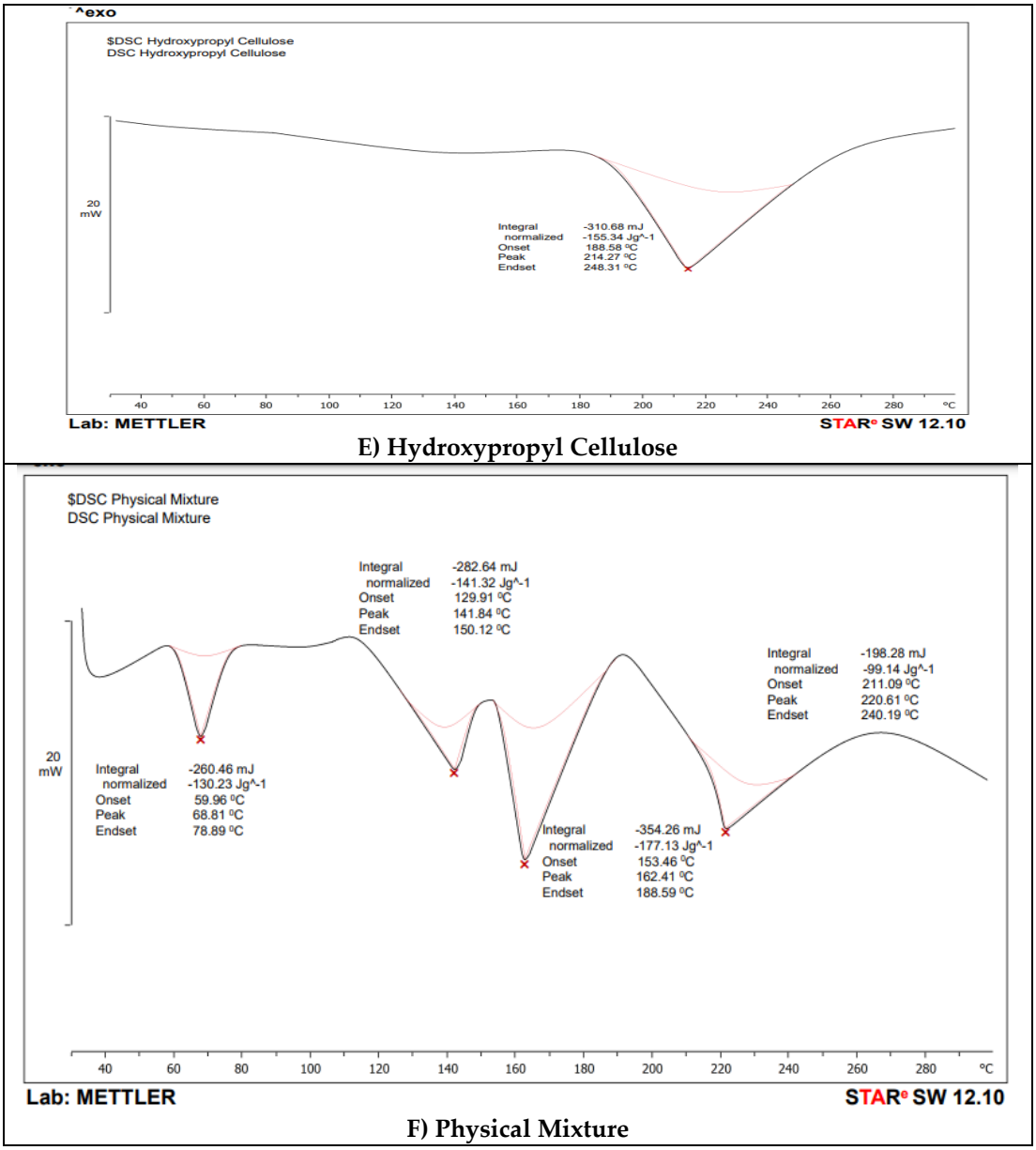



**Figure 1.** DSC thermograms of Drug, Excipients and Physical Mixture

### 3.3 FTIR Spectroscopic Analysis

FTIR spectroscopy was performed to investigate the chemical compatibility of luliconazole with the selected formulation excipients and to identify any potential drug–excipient interactions in the physical mixture (Figure 2). The FTIR spectrum of pure luliconazole exhibited characteristic absorption bands corresponding to its major functional groups. The prominent peaks observed at 3060–3020 $cm^{-1}$ were assigned to aromatic C–H stretching vibrations, while the bands within 2950–2850 $cm^{-1}$ corresponded to aliphatic C–H stretching vibrations. The absorption band observed around 2235–2220 $cm^{-1}$ was attributed to nitrile (C≡N) stretching vibration, whereas the peak near 1645 $cm^{-1}$ was associated with characteristic aromatic ring and heterocyclic stretching vibrations. Additional bands in the region of 1450–1380 $cm^{-1}$ corresponded to C–H bending vibrations, while peaks between 1250–1050 $cm^{-1}$ were attributed to C–O–C, C–N, and imidazole ring-associated stretching vibrations. The presence of these characteristic absorption bands confirmed the chemical integrity and structural identity of luliconazole.

The FTIR spectra of individual excipients showed their characteristic functional group vibrations. HPMC exhibited a broad absorption band around 3425 $cm^{-1}$ due to hydroxyl (O–H) stretching, along with C–H

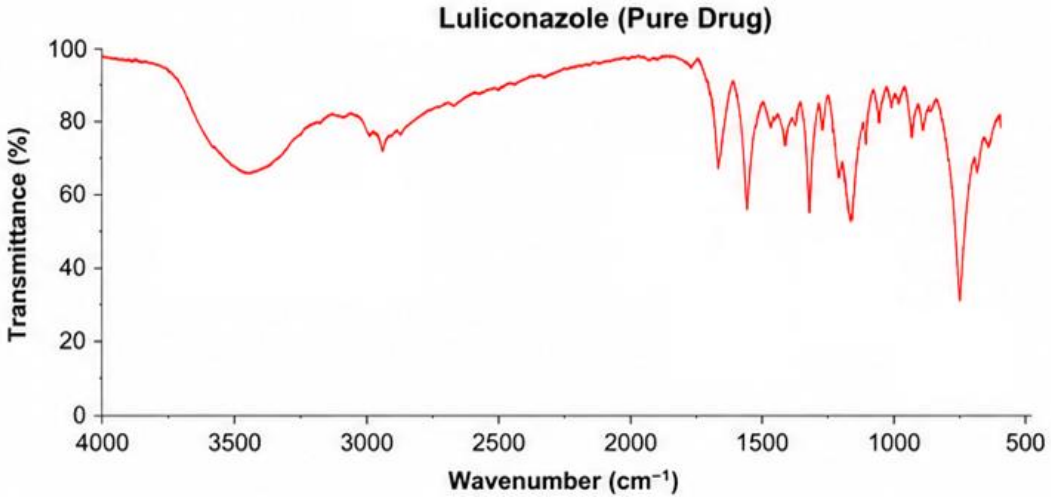
DOI: https://doi.org/10.66220/qap0cz96 ISSN: 3139-9258

stretching near 2920 $cm^{-1}$ and C–O–C stretching around 1055 $cm^{-1}$, representing its cellulose ether structure. PEG 400 showed a broad hydroxyl stretching band around 3400 $cm^{-1}$, aliphatic C–H stretching vibrations between 2880–2950 $cm^{-1}$, and a strong ether C–O–C stretching band near 1100 $cm^{-1}$. The spectrum of Eudragit RS-100 demonstrated characteristic polymeric vibrations, including broad O–H stretching around 3430 $cm^{-1}$, ester carbonyl (C=O) stretching near 1725 $cm^{-1}$, aliphatic C–H stretching between 2950–2870 $cm^{-1}$, and ester C–O–C stretching bands within 1140–1260 $cm^{-1}$. Similarly, Hydroxypropyl Cellulose (HPC) exhibited a broad O–H stretching band around 3460 $cm^{-1}$, C–H stretching near 2920 $cm^{-1}$, and strong C–O/C–O–C stretching vibrations around 1100 $cm^{-1}$. These spectral characteristics corresponded well with the reported functional group vibrations of the respective excipients.

The FTIR spectrum of the physical mixture showed the retention of the characteristic absorption bands of luliconazole along with the prominent peaks of the incorporated excipients. The characteristic drug-associated peak near 1645 $cm^{-1}$ was retained and observed around 1650 $cm^{-1}$, showing only a minor shift (~5 $cm^{-1}$). The broad hydroxyl stretching region (3450–3550 $cm^{-1}$) showed increased intensity and broadening due to the overlapping of hydroxyl vibrations from hydrophilic polymers such as HPMC, HPC, and PEG 400. Importantly, no disappearance of luliconazole-specific absorption bands, generation of new peaks, or significant alteration of functional group vibrations was observed in the physical mixture.

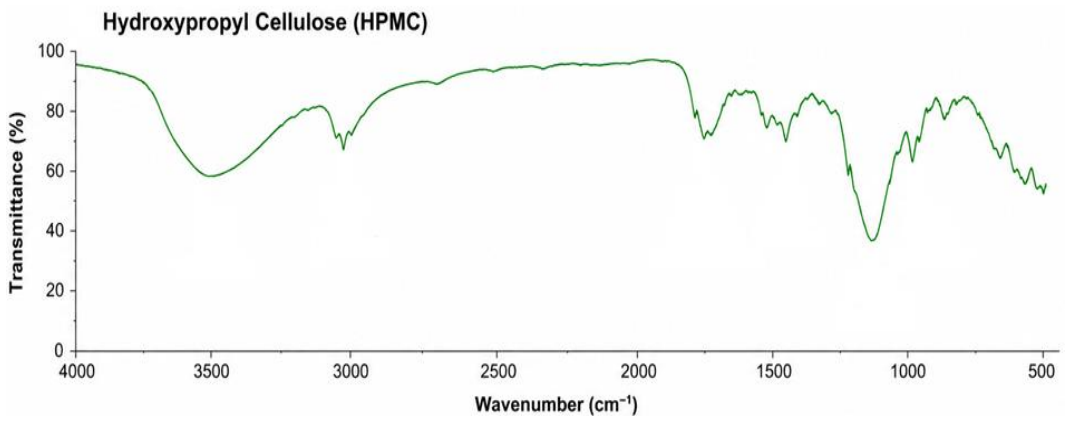
The minor variations in peak positions and broadening of hydroxyl absorption bands may be attributed to physical mixing, changes in the molecular environment, and weak intermolecular interactions, particularly hydrogen bonding between the drug and polymeric excipients. However, the absence of substantial peak shifts (>10 $cm^{-1}$), new absorption bands, or modification of characteristic imidazole-related vibrations indicates the absence of chemical interaction, covalent bond formation, or degradation of luliconazole. Additionally, the absence of any additional carbonyl absorption bands confirms that no chemical transformation, such as esterification or oxidative degradation, occurred during mixing.

Overall, FTIR analysis confirmed that the characteristic functional groups and chemical structure of luliconazole were preserved in the presence of HPMC, HPC, PEG 400, and Eudragit RS-100. The observed minor spectral changes were attributed to physical interactions and weak hydrogen bonding rather than chemical incompatibility. These findings demonstrate the excellent compatibility of luliconazole with the selected excipients, supporting their suitability for further formulation development.

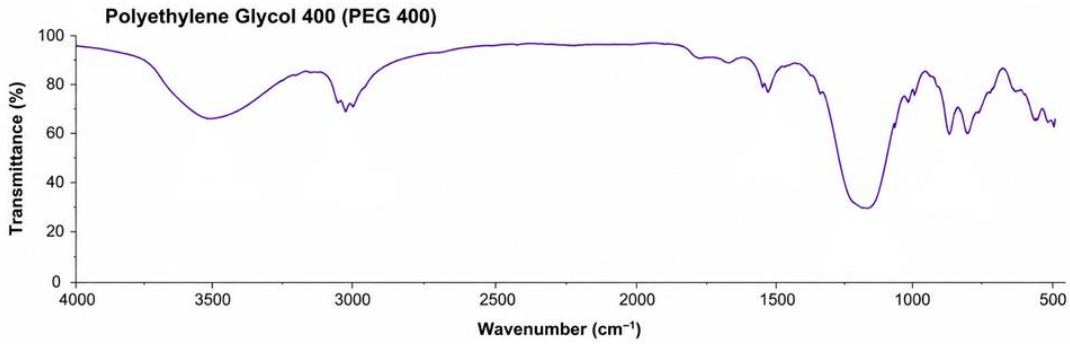



**A) Luliconazole**

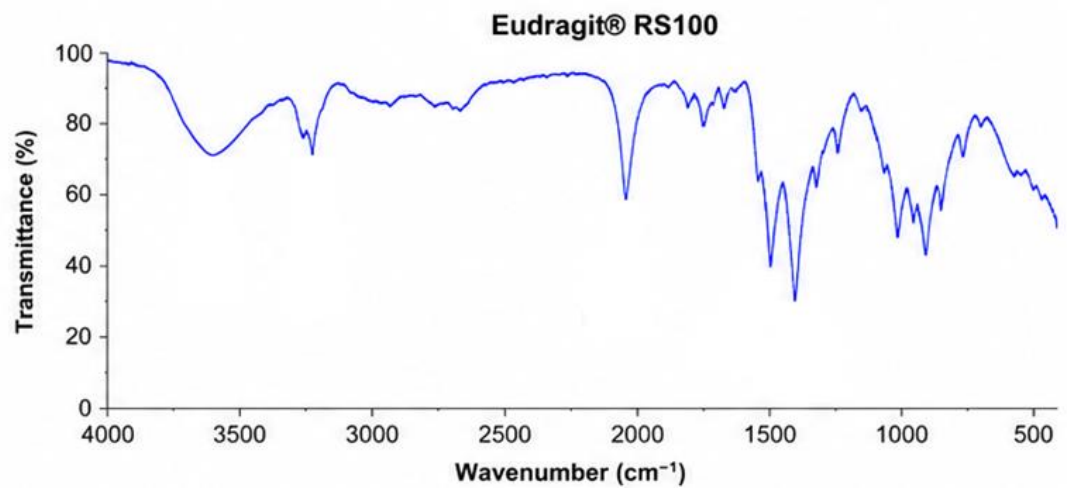
DOI: https://doi.org/10.66220/qap0cz96 ISSN: 3139-9258




**B) HPMC**




**C) PEG 400**




**D) Eudragit RS-100**

DOI: https://doi.org/10.66220/qap0cz96 ISSN: 3139-9258

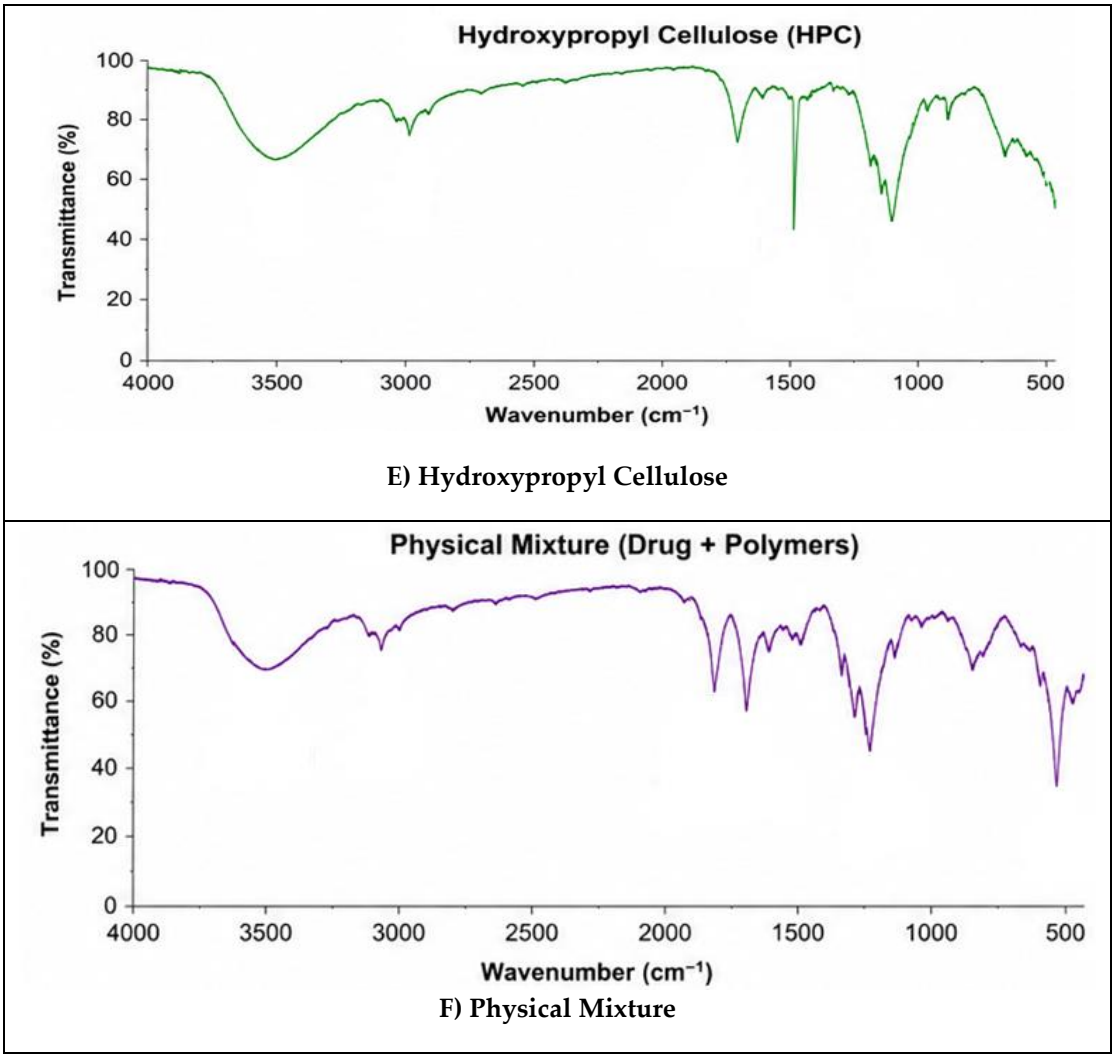



**Figure 2.** FTIR graphs of Drug, Excipients and Physical Mixture

### 3.4 Solubility Determination (Shake Flask Method)

The equilibrium solubility of luliconazole was determined using the shake-flask method at 37 ± 0.5°C, and the results obtained from triplicate measurements are presented as mean ± SD (n = 3) in Table 2 and Figure 3. The solubility profile demonstrated a pronounced difference between the aqueous and organic solvent systems, indicating the highly lipophilic and poorly water-soluble nature of luliconazole.

Luliconazole exhibited extremely low aqueous solubility in distilled water (0.003 ± 0.001 mg/mL), suggesting limited dissolution under neutral aqueous conditions. Similarly, poor solubility was observed in 0.1 N HCl (pH 1.2) (0.005 ± 0.002 mg/mL), phosphate buffer pH 6.8 (0.007 ± 0.003 mg/mL), and phosphate buffer pH 7.4 (0.009 ± 0.006 mg/mL). The slightly increased solubility observed at higher pH values may be associated with the ionization behavior of the drug; however, the overall solubility remained insufficient due to its predominantly hydrophobic molecular structure.

In contrast, luliconazole showed significantly enhanced solubility in organic solvents, with the highest solubility observed in methanol (48.76 ± 0.84 mg/mL), followed by ethanol (26.43 ± 0.61 mg/mL). The improved solubility in these solvents can be attributed to favorable solvent–drug interactions, including hydrogen bonding and hydrophobic interactions, which facilitate disruption of the drug crystal lattice and improve molecular dispersion. The higher solubility in methanol compared with ethanol may be due to its greater polarity and stronger solvation capacity toward the functional groups present in luliconazole.

The observed poor aqueous solubility is consistent with the physicochemical characteristics of luliconazole, which possesses a highly aromatic and halogenated structure that contributes to strong intermolecular crystal packing and high lipophilicity. Such characteristics result in limited wettability and dissolution in aqueous environments, which may potentially restrict its bioavailability and therapeutic performance when conventional formulations are used.

The low standard deviation values observed across all experimental conditions indicate good reproducibility, precision, and reliability of the shake-flask solubility assessment. Based on the obtained solubility profile, methanol demonstrated the highest solubilizing capacity; however, considering formulation applicability and safety aspects, ethanol and suitable solubilization approaches may be explored for developing an optimized delivery system.

Overall, the solubility study confirmed the poor aqueous solubility of luliconazole and its preference for organic solvents, highlighting the need for formulation strategies such as lipid-based systems, polymeric carriers, or nanoformulations to enhance drug solubility and dissolution characteristics.

**Table 2.** Solubility studies of Luliconazole

| Solvent | Luliconazole |
|---|---|
| | Solubility in mg/mL (Mean ± SD) |
| **Distilled Water** | 0.003 ± 0.001 |
| **0.1 N HCl (pH 1.2)** | 0.005 ± 0.002 |
| **Phosphate Buffer pH 6.8** | 0.007 ± 0.003 |
| **Phosphate Buffer pH 7.4** | 0.009 ± 0.006 |
| **Methanol** | 48.76 ± 0.84 |
| **Ethanol** | 26.43 ± 0.61 |

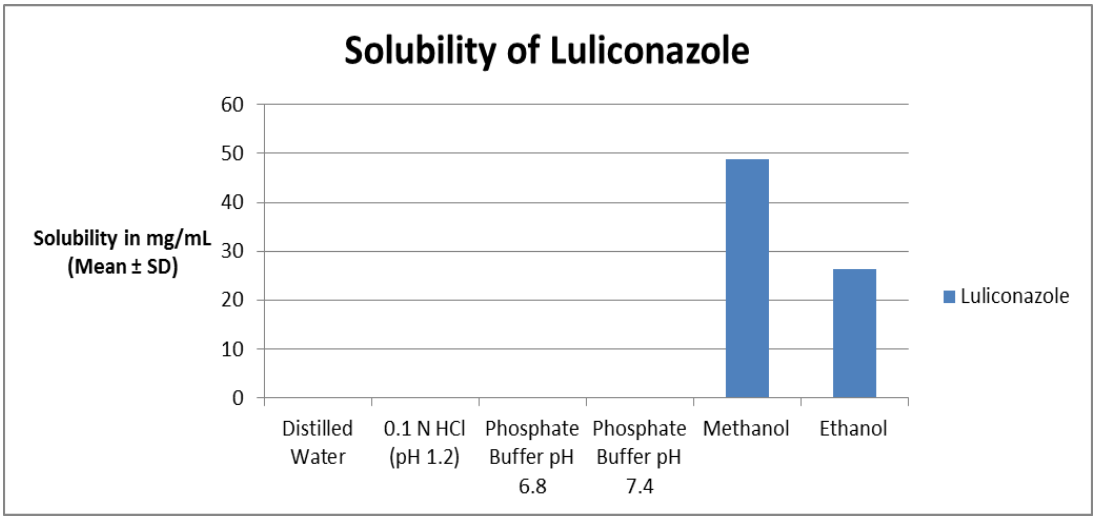



**Figure 3.** The graphical representations (Mean ± SD, n = 3) for solubility of drug

### 3.5 UV–Visible Spectroscopic Analysis

UV–visible spectrophotometric analysis was performed to determine the absorption maximum (λmax) of luliconazole in methanol as part of the preformulation characterization (Figure 4). Methanol was selected because of its excellent solubilizing ability and negligible interference in the UV region.

The UV spectrum of luliconazole exhibited a distinct absorption maximum at λmax = 296 nm, attributed to π→π* electronic transitions of aromatic and imidazole chromophores present in the drug structure. The observed λmax was consistent with reported values, confirming the identity and chemical integrity of luliconazole. The absence of additional peaks indicated no degradation during analysis. Thus, 296 nm was

DOI: https://doi.org/10.66220/qap0cz96 ISSN: 3139-9258

selected as a suitable analytical wavelength for reliable quantification of luliconazole in subsequent preformulation and formulation studies.

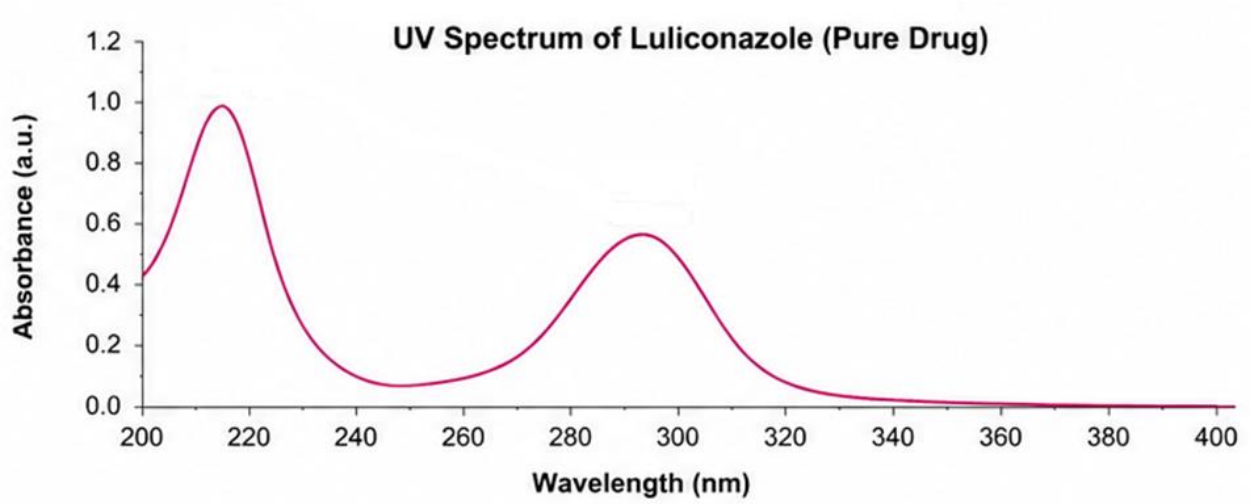



**Figure 4.** The UV Visible graphs of Luliconazole

### 3.6 Construction of Calibration Curve

The calibration curve of luliconazole was developed in methanol at λmax = 296 nm over a concentration range of 2–20 µg/mL using triplicate measurements (n = 3). The experimental absorbance values and statistical analysis are presented in Table 3, while the corresponding calibration plot is shown in Figure 5.

Table 3 shows a gradual increase in absorbance with increasing concentrations of Luliconazole. At the lowest concentration of 2 µg/mL, the mean absorbance was 0.085 ± 0.0010, which increased proportionally to 0.859 ± 0.0020 at the highest concentration of 20 µg/mL. The intermediate concentrations also showed a consistent increase in absorbance, confirming the concentration-dependent response of the drug in the methanolic medium.

The calibration data showed excellent linearity throughout the selected concentration range. Regression analysis of absorbance versus concentration resulted in a correlation coefficient ($R^2$ = 0.9998), indicating a strong positive linear relationship between the Luliconazole concentration and absorbance. The low standard deviation values (0.0010–0.0020) observed for all concentrations indicate minimal variation among replicate measurements, confirming the precision and reproducibility of the analytical method.

**Table 3.** The calibration curve results at concentration range of 2–20 µg/mL (n = 3)

| Concentration (µg/mL) | Luliconazole (296 nm) | | | |
|---|---|---|---|---|
| | 1 | 2 | 3 | Mean ± SD |
| **2** | 0.084 | 0.086 | 0.085 | 0.085 ± 0.0010 |
| **4** | 0.171 | 0.173 | 0.172 | 0.172 ± 0.0010 |
| **6** | 0.256 | 0.259 | 0.258 | 0.258 ± 0.0015 |
| **8** | 0.343 | 0.345 | 0.344 | 0.344 ± 0.0010 |
| **10** | 0.429 | 0.431 | 0.430 | 0.430 ± 0.0010 |
| **12** | 0.514 | 0.517 | 0.516 | 0.516 ± 0.0015 |
| **14** | 0.600 | 0.603 | 0.688 | 0.602 ± 0.0015 |
| **16** | 0.686 | 0.689 | 0.960 | 0.688 ± 0.0015 |
| **18** | 0.772 | 0.775 | 0.774 | 0.774 ± 0.0015 |
| **20** | 0.857 | 0.861 | 0.859 | 0.859 ± 0.0020 |
| **Correlation coefficient: $R^2$** | | | 0.9998 | |

The obtained results confirm that Luliconazole follows Beer–Lambert's law within the concentration range of 2–20 µg/mL in methanol. The developed calibration curve exhibited high linearity, accuracy, and precision, making it suitable for routine quantitative estimation of Luliconazole during preformulation and formulation evaluation studies. The established analytical method provides a reliable basis for subsequent drug content determination and dissolution studies.

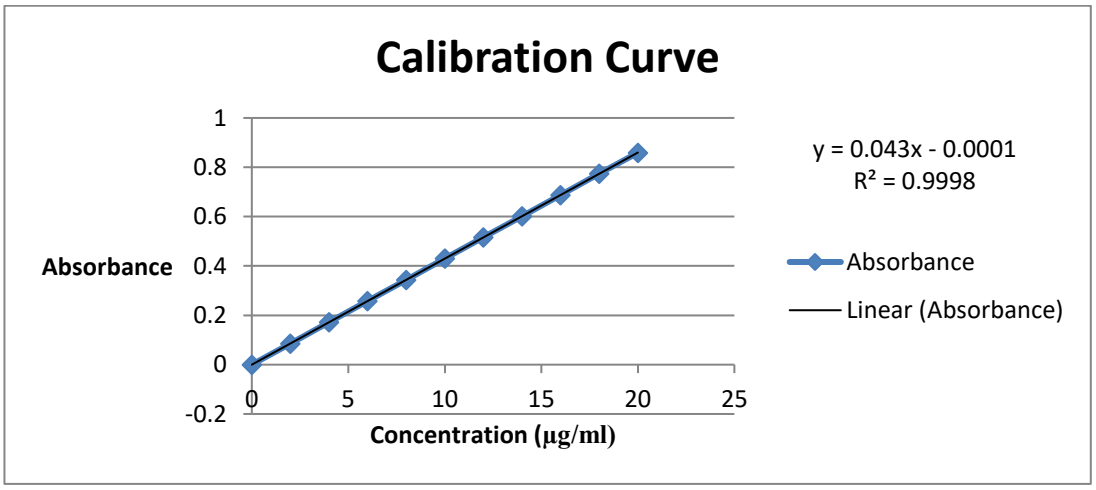



**Figure 5.** Calibration curve of Luliconazole in methanol

### 3.7 Formulation of combined spray formulation dosage form by QBD approach

#### *3.7.1 Statistical Design of experiments (DOE)*

A $2^3$ full factorial design was employed for the development and optimization of a topical film-forming antifungal and steroidal spray containing luliconazole. The concentrations of Hydroxypropyl Cellulose (HPC) (A, % w/v), Eudragit® RS100 (B, % w/v), and PEG 400 (C, % v/v) were selected as independent variables and evaluated at two levels (-1 and +1). The effects of these formulation variables on the drying time ($Y_1$) and viscosity of the formed film ($Y_2$) were investigated as dependent variables, as shown in Table 4.

#### *3.7.2 Preparation of Luliconazole Film-Forming Spray*

A series of eight Luliconazole film-forming spray formulations (F1–F8) were successfully prepared by varying the concentrations of formulation variables A, B, and C, and their effects on film formation time ($Y_1$) and viscosity ($Y_2$) were evaluated. All formulations appeared clear and homogeneous without visible precipitation, indicating satisfactory physical compatibility of the formulation components.

As presented in Table 4, the film formation time ranged from 3.8 to 8.2 min, whereas the viscosity varied between 162 and 438 cP. Formulation F4 exhibited the shortest film formation time (3.8 min), while F2 required the longest time (8.2 min). The highest viscosity was observed for F3 (438 cP), whereas F6 showed the lowest viscosity (162 cP).

The observed variations indicate that changes in the formulation composition influenced both film formation time and viscosity. Formulations with comparatively higher viscosity generally required a longer time to form a continuous film, which may be attributed to slower solvent evaporation and increased polymer chain interactions. Overall, all formulations exhibited acceptable film-forming behavior and viscosities suitable for spray application, demonstrating that the selected composition range was appropriate for further optimization.

**Table 4.** Design Batches

| Formulation Code | A (%) | B (%) | C (%) | $Y_1$ (Min) | $Y_2$ (CP) |
|---|---|---|---|---|---|
| **F1** | 2 | 2 | 5 | 5.6 | 295 |

DOI: https://doi.org/10.66220/qap0cz96 ISSN: 3139-9258

| | | | | | |
|---|---|---|---|---|---|
| **F2** | 2 | 4 | 10 | 8.2 | 412 |
| **F3** | 2 | 4 | 5 | 6.9 | 438 |
| **F4** | 1 | 2 | 5 | 3.8 | 178 |
| **F5** | 2 | 2 | 10 | 6.8 | 278 |
| **F6** | 1 | 2 | 10 | 5.2 | 162 |
| **F7** | 1 | 4 | 10 | 6.4 | 286 |
| **F8** | **1** | **4** | **5** | **5.1** | **304** |

### 3.8 Optimization data analysis and model-validation

The factor effects and corresponding p-values for the response variables are shown in Table 5. Different mathematical models, such as mean, two-factor interaction (2FI), and main effect, were utilized to analyze the results derived from the study. To further investigate the intricate correlations between the independent and response variables, a 3D response surface plot was used.

**Table 5.** Summary of results of regression analysis for responses $Y_1$ and $Y_2$

| Models | $R^2$ | Adjusted $R^2$ | Predicted $R^2$ | SD | %CV |
|---|---|---|---|---|---|
| **Response ($Y_1$) Main Effect** | 0.9988 | 0.9980 | 0.9953 | 0.0612 | 1.02 |
| **Response ($Y_2$) Main Effect** | 0.9981 | 0.9967 | 0.9926 | 5.53 | 1.88 |

**Regression Equations**

$$Y1=6.00+0.8750A+0.6500B+0.6500C\text{---------- (13)}$$
$$Y2=294.13+61.62A+65.88B-9.63C\text{---------- (14)}$$

#### *3.8.1 Model Assessment for Dependent Variables*

After putting the data in Design Expert® software for, Fit summary applied to data in that main effect model was suggested by the software for all the responses. The statistical evaluation was performed using ANNOVA. Results are shown in (Table 6 and 7). The coefficients with more than one factor term in the regression equation represent the interaction terms. It also shows that the relationship between factors and responses is not always linear. When more than one factor is changed simultaneously and used at different levels in a formulation, a factor can produce different degrees of responses.

**Table 6.** Results of Analysis of Variance for Measured Response (Y1)

| Source | Sum of Squares | df | Mean Square | F-value | p-value | |
|---|---|---|---|---|---|---|
| **Model** | 12.88 | 3 | 4.29 | 1145.33 | < 0.0001 | |
| **A-HPC** | 6.12 | 1 | 6.12 | 1633.33 | < 0.0001 | |
| **B-Eudragit® RS100** | 3.38 | 1 | 3.38 | 901.33 | < 0.0001 | **Significant** |
| **C-PEG 400** | 3.38 | 1 | 3.38 | 901.33 | < 0.0001 | |
| **Residual** | 0.0150 | 4 | 0.0037 | | | |
| **Cor Total** | 12.90 | 7 | | | | |

**Table** Error! No text of specified style in document.. Results of Analysis of Variance for Measured Response (Y2)

| Source | Sum of Squares | df | Mean Square | F-value | p-value | |
|---|---|---|---|---|---|---|
| **Model** | 65838.38 | 3 | 21946.13 | 716.61 | < 0.0001 | |
| **A-HPC** | 30381.12 | 1 | 30381.12 | 992.04 | < 0.0001 | |
| **B-Eudragit® RS100** | 34716.12 | 1 | 34716.12 | 1133.59 | < 0.0001 | **Significant** |
| **C-PEG 400** | 741.13 | 1 | 741.13 | 24.20 | 0.0079 | |
| **Residual** | 122.50 | 4 | 30.62 | | | |

DOI: https://doi.org/10.66220/qap0cz96 ISSN: 3139-9258

| | | |
|---|---|---|
| **Cor Total** | 65960.88 | 7 |

### *3.8.2 Response Surface Plot Analysis*

3D response surface plots were generated using Design Expert® software and are presented in Figures 6 and 7 for the studied responses, i.e., drying time (min) ($Y_1$) and viscosity (CP) ($Y_2$).

The response surface plots indicated that increasing the concentrations of HPC and Eudragit® RS100 increased both drying time and viscosity due to the formation of a denser polymeric matrix. PEG 400 slightly increased the drying time while reducing viscosity because of its plasticizing effect. Among the formulation variables, HPC had the greatest influence on both responses.

Based on the optimization criteria, formulation F8 (1% w/v HPC, 4% w/v Eudragit® RS100, and 5% v/v PEG 400) was selected as the optimized batch, exhibiting a drying time of 5.1 min and viscosity of 304 cP. The formulation showed good sprayability and formed a uniform, flexible, and adherent film suitable for topical application.

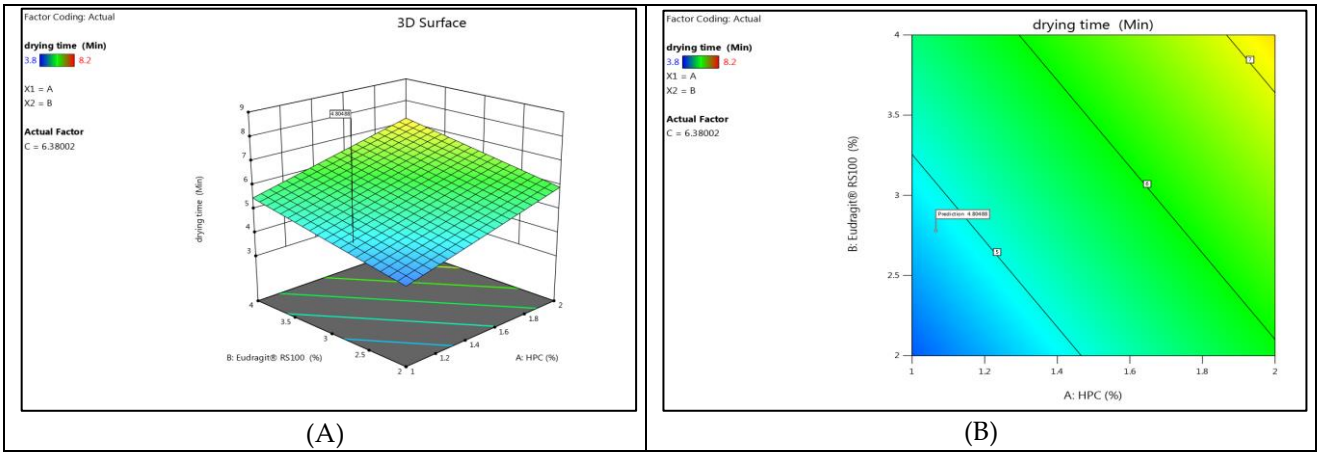



**Figure 1.** (A) 3D Surface Plot (B) Contour Plot of Drying Time

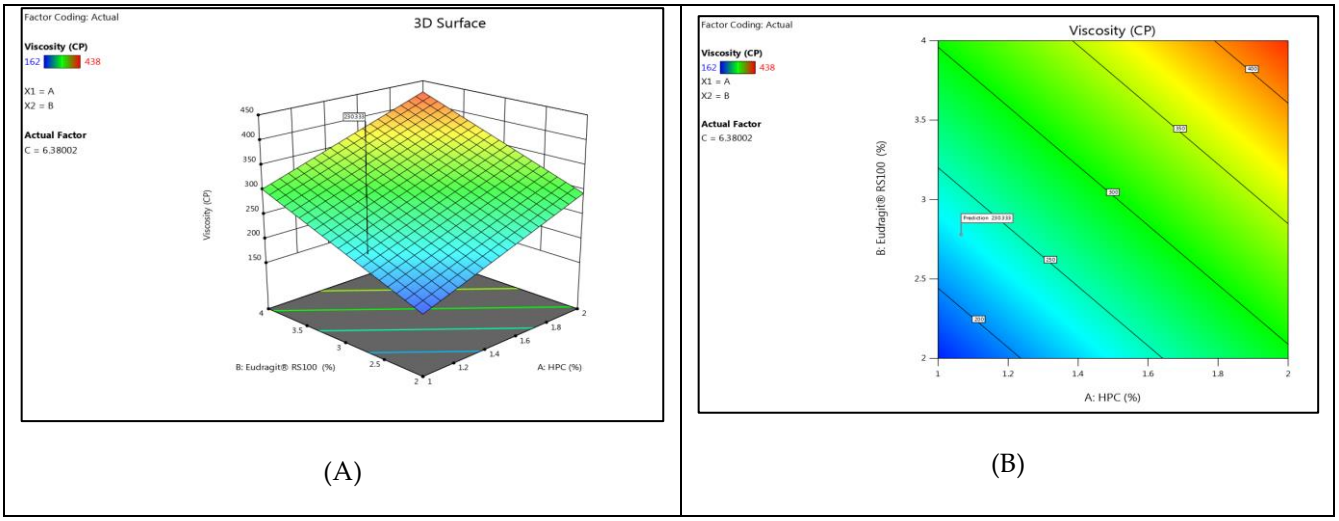



**Figure 7.** (A) 3D Surface Plot (B) Contour Plot of Drying Time of Viscosity

The main effect model demonstrated significant results with a p-value less than 0.05. An ANOVA test was conducted, and the results were significant.

**Table 8.** Formulation Table of Optimized Batch (F8)

| Ingredients | Quantity (100ml) |
|---|---|
| **Luliconazole** | 1000mg (1%) |
| **Hydroxypropyl Cellulose (HPC)** | 1gm (1%) |
| **Eudragit® RS100** | 4gm (4%) |
| **PEG 400** | 5ml (5%) |
| **Ethanol** | 70ml |
| **Water** | Q.S. to 100ml |

### 3.9 Evaluation of Spray Formulation

#### *3.9.1 Appearance and Film Formation*

All formulations were clear, homogeneous, and free from visible particulate matter, producing transparent and smooth films. Formulations with higher polymer concentrations exhibited improved film integrity and adhesion. Among all batches, F8 showed the best film-forming characteristics, producing a uniform, transparent, non-sticky, and adherent film with an acceptable drying time and sprayability.

#### *3.9.2 Viscosity*

The viscosity of the formulations ranged from 162 to 438 cP and increased with increasing concentrations of HPMC and sodium alginate, as shown in Table 9.

**Table 9.** Evaluation of Spray Formulation

| Batch | pH | Viscosity (cp) | Evaporation time | Spray angle (%) |
|---|---|---|---|---|
| **F1** | 6.42 ± 0.03 | 295 ± 4 | 5.6 ± 0.18 | 79.2 ± 0.62 |
| **F2** | 6.38 ± 0.04 | 412 ± 6 | 8.2 ± 0.21 | 66.5 ± 0.58 |
| **F3** | 6.46 ± 0.02 | 438 ± 5 | 6.9 ± 0.19 | 64.8 ± 0.55 |
| **F4** | 6.50 ± 0.03 | 178 ± 3 | 3.8 ± 0.14 | 89.6 ± 0.70 |
| **F5** | 6.55 ± 0.04 | 278 ± 4 | 6.8 ± 0.20 | 80.5 ± 0.60 |
| **F6** | 6.58 ± 0.03 | 162 ± 3 | 5.2 ± 0.16 | 86.8 ± 0.65 |
| **F7** | 6.63 ± 0.02 | 286 ± 4 | 6.4 ± 0.18 | 78.4 ± 0.54 |
| **F8** | 6.51 ± 0.02 | 304 ± 5 | 5.1 ± 0.15 | 83.6 ± 0.61 |

#### *3.9.3 pH*

The pH of all formulations ranged between 6.38 ± 0.04 and 6.63 ± 0.02, and the results are shown in Table 9, which is in accordance with the pH of the skin, indicating compatibility with the skin's natural pH.

#### *3.9.4 Evaporation time*

The evaporation (drying) time varied from 3.8 to 8.2 min, with higher polymer concentrations resulting in prolonged drying due to increased solvent retention within the polymeric matrix. Formulation F4 exhibited the shortest drying time (3.2 min), whereas formulation F2 showed the longest drying time (8.3 min), as shown in Table 9.

#### *3.9.5 Spray angle*

The spray angle of the formulations ranged from 64.8° to 86.8°. Formulations with lower viscosity exhibited larger spray angles, indicating better atomization and wider spray distribution, whereas highly viscous formulations showed reduced spray angles owing to increased resistance to flow through the spray nozzle, as shown in Table 9. Among all batches, formulation F8 demonstrated optimum film-forming properties

with a viscosity of 304 cP, drying time of 5.1 min, and spray angle of 83.6°, producing a uniform, transparent, non-sticky, and adherent film suitable for topical application.

### 3.10 Evaluation of Film

#### *3.10.1 Thickness of the films*

The film thickness ranged from 0.15±0.01 to 0.29±0.02 mm, with higher polymer concentrations producing thicker films due to increased matrix formation, as shown in Table 10.

#### *3.10.2 Film Flexibility (Folding Endurance)*

The folding endurance values ranged from 96±3 to 145±5, demonstrating satisfactory flexibility and mechanical strength of the films. Formulations containing higher concentrations of HPC and Eudragit® RS100 exhibited greater folding endurance owing to enhanced polymer chain interactions, as shown in Table 10.

**Table 10.** Evaluation of Film

| Batch | Thickness (mm) | Folding endurance | Stickiness | Washability & Leak Test |
|---|---|---|---|---|
| **F1** | 0.20±0.01 | 118±3 | Slightly Sticky | Pass |
| **F2** | 0.27±0.02 | 140±4 | Sticky | Pass |
| **F3** | 0.29±0.02 | 145±5 | Sticky | Pass |
| **F4** | 0.15±0.01 | 96±3 | Non-Sticky | Pass |
| **F5** | 0.19±0.01 | 112±2 | Non-Sticky | Pass |
| **F6** | 0.16±0.01 | 101±2 | Non-Sticky | Pass |
| **F7** | 0.22±0.01 | 120±3 | Slightly Sticky | Pass |
| **F8** | 0.21±0.01 | 128±3 | Non-Sticky | Pass |

#### *3.10.3 Stickiness of the film*

Stickiness evaluation revealed that formulations with higher polymer content showed slight to moderate stickiness, whereas formulations with lower polymer concentrations produced non-sticky films.

#### *3.10.4 Washability and leak test*

All formulations successfully passed the washability and leak tests, indicating good adhesion and integrity of the formed films upon application.

#### *3.10.5 Drug content*

The drug content for F8 formulations is found to be within the range of 99.2±0.8% as shown in Table 11. This indicates that the formed film had a uniform distribution of drug.

**Table 11**. Drug Content of F8

| | F8 Batch |
|---|---|
| **Luliconazole** | 99.2±0.8% |

#### *3.10.6 In-vitro diffusion study using eggshell membrane (In-vitro drug release)*

The *in vitro* diffusion study of the optimized formulation (F8) was performed using an eggshell membrane in a Franz diffusion cell to evaluate the release behavior of Luliconazole. The formulation exhibited a gradual and sustained diffusion pattern for the drug over a period of 8 h. Luliconazole showed an initial diffusion of 15.74% at 1 h, which progressively increased to 67.36% at 4 h and reached 98.18% at 8 h. The results

DOI: https://doi.org/10.66220/qap0cz96 ISSN: 3139-9258

indicate that the optimized formulation provided efficient and nearly complete drug diffusion within 8 h, demonstrating its potential for effective topical delivery of Luliconazole, as shown in Table 12 and Figure 8.

**Table 12**. In-vitro drug release

| Time (Hours) | F8 %CDR Luliconazole |
|---|---|
| **0** | 0 |
| **1** | 15.74 |
| **2** | 24.74 |
| **3** | 43.5 |
| **4** | 67.36 |
| **5** | 84.43 |
| **8** | 98.18 |

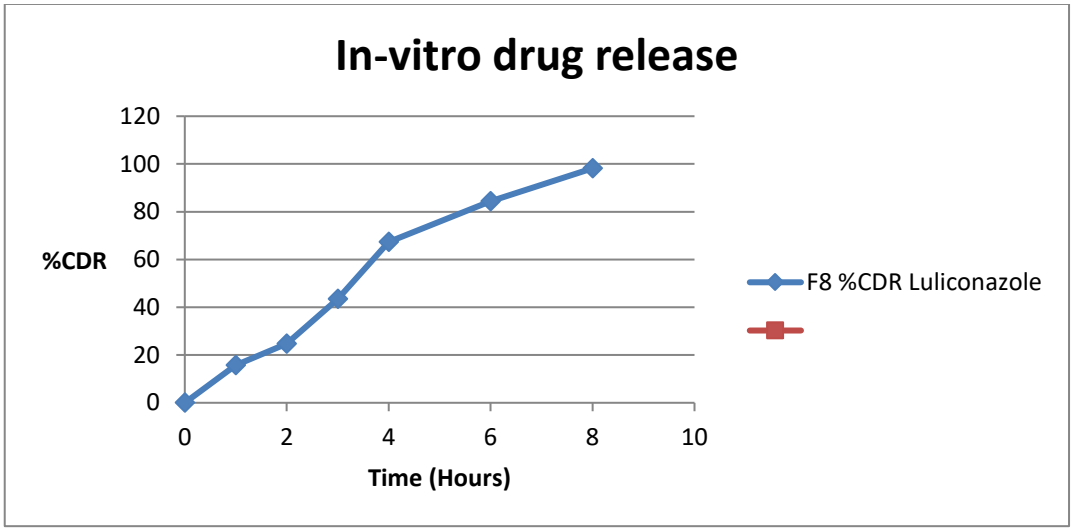



**Figure 2.** In-vitro drug release

### 3.11 Kinetics of drug release

The release kinetics of the optimized formulation (F8) were analyzed using various kinetic models. For luliconazole, the highest $R^2$ values were obtained using the Hixson–Crowell model (0.9724), indicating that drug release was governed by changes in the surface area and dimensions of the polymeric film during diffusion. The zero-order model also showed good correlation, whereas the first-order, Higuchi, and Korsmeyer–Peppas models exhibited comparatively lower $R^2$ values. These results suggest that the optimized film-forming spray provided controlled drug release through a combination of diffusion and gradual matrix erosion, as shown in Table 13 and Figure 9.

**Table 13.** $R^2$ values of various Kinetic Models

| Kinetic Model | $R^2$ Value (Luliconazole) |
|---|---|
| **Zero order release kinetics** | 0.9667 |
| **First order release kinetics** | 0.8956 |
| **Higuchi release kinetics** | 0.9218 |
| **Korsemeyer Peppas release kinetics** | 0.7003 |
| **Hixon Crowell release kinetics** | 0.9723 |

DOI: https://doi.org/10.66220/qap0cz96 ISSN: 3139-9258

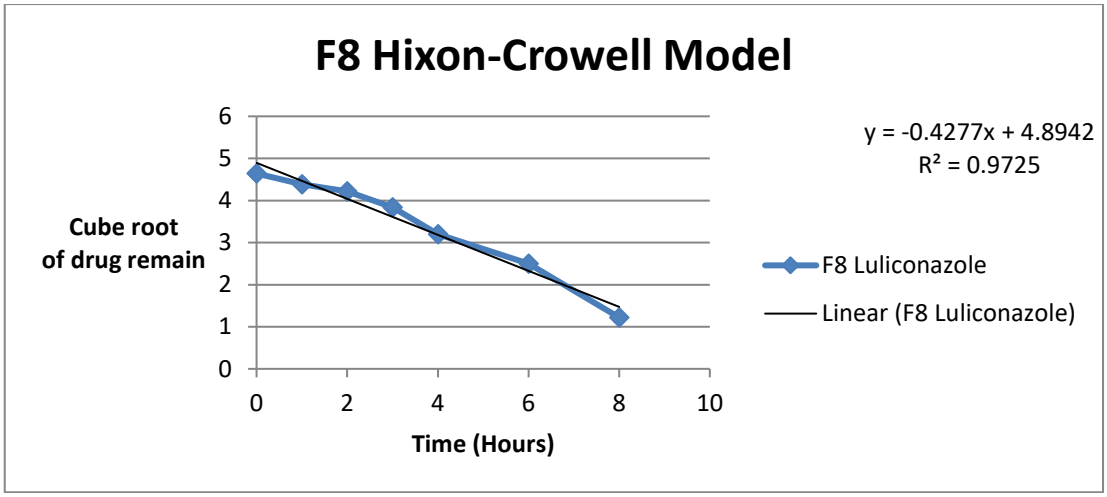



**Figure 3.** Kinetics of F8

### 3.12 Accelerated Stability Study

The optimized formulation (F8) was subjected to accelerated stability testing to evaluate its physicochemical stability under accelerated storage conditions. The results are presented in Table 14.

Throughout the 3-month study period, formulation F8 remained clear and homogeneous, with no visible signs of precipitation, phase separation, or color change, indicating good physical stability. The pH values showed only minor fluctuations, ranging from 6.15 ± 0.03 to 6.51 ± 0.02, while the viscosity remained relatively constant between 304 ± 5 and 310 ± 3 cP. These variations were minimal and within acceptable limits, suggesting that storage under accelerated conditions did not significantly affect the formulation characteristics.

Overall, the accelerated stability study demonstrated that the optimized formulation F8 maintained its physical appearance, pH, and viscosity throughout the study period, confirming its satisfactory stability and suitability for storage under the tested conditions.

**Table 14.** Stability study of parameters of the optimized formulation (F8)

| Parameters | Initial Month | 1st Month | 2nd Month | 3rd Month |
|---|---|---|---|---|
| **Appearance** | Clear, homogeneous solution | | | |
| **pH** | 6.51±0.02 | 6.23±0.02 | 6.15±0.03 | 6.49±0.04 |
| **Viscosity (cP)** | 304±5 | 310±3 | 306±2 | 308±4 |

## 4. Conclusion

The present study successfully demonstrated the development and optimization of a Luliconazole film-forming topical spray using a Quality by Design (QbD) approach. A (2^3) full factorial design was effectively employed to investigate the influence of hydroxypropyl cellulose (HPC), Eudragit® RS100, and PEG 400 on critical formulation responses, particularly drying time and viscosity. The systematic formulation approach enabled the identification of an optimized formulation with desirable physicochemical and performance characteristics. Among the developed formulations, F8 exhibited a drying time of 5.1 min and viscosity of 304 cP, indicating suitable properties for topical application and film formation. The formulation was further evaluated for appearance, pH, spray characteristics, film properties, drug content, and in vitro drug diffusion. The QbD-based optimization strategy provided a structured and efficient approach for understanding formulation variables and achieving the desired product characteristics. Overall, the developed Luliconazole film-forming spray represents a promising topical drug-delivery system with potential advantages in terms of ease of application and formation of a drug-containing film at the site of administration. Further studies may be warranted to establish its long-term stability and performance under in vivo conditions.

**Acknowledgments**

None

**Conflict of Interest**

"The authors declare no conflict of interest."

**Authors' Contribution**

A.G. and M.P.; methodology, A.G.; software, A.G.; validation, A.G., A.P and formal analysis, A.G.; investigation, A.G.; resources, A.G.; data curation, A.G.; writing—original draft preparation, A.G.; writing—review and editing, A.G.; visualization, A.G.; supervision, A.G.; project administration, A.G.; funding acquisition, M.P. All authors have read and agreed to the published version of the manuscript." Authorship must be limited to those who have contributed substantially to the work reported.

**Funding**

"This research received no external funding"

## References

1. Shi G, Guo Y, Yang M. Development and optimization of a novel nanocarrier SabiWhite-loaded ethosomal gel for targeted skin inflammation complicated by multidrug-resistant pathogens. Front Cell Infect Microbiol. 2025;15. doi: 10.3389/fcimb.2025.1640799.
2. Zhu Z, Li W, Yin Y, Cao R, Li Z. Differential Scanning Calorimetry Material Studies: Benzil Melting Point Method for Eliminating the Thermal History of DSC. Vol. 2022, Journal of Chemistry. 2022. doi: 10.1155/2022/3423429.
3. Shaligram PS, George CP, Sharma H, Mahadik KR, Patil S, Vanka K, et al. Rivaroxaban eutectics with improved solubility, dissolution rates, bioavailability and stability. CrystEngComm. 2023;25(22):3253–63. doi: 10.1039/d3ce00261f.
4. Liaqat R, Rasool F, Noreen S, Rai N, Naseem A, Shoaib MH, et al. Fabrication, characterization, and docking studies of furosemide-loaded nanosponges using the emulsion solvent diffusion method. Nanomedicine. 2025;20(11):1235–47. doi: 10.1080/17435889.2025.2501518.
5. Chaudhari Rn, L.Khan S, Chaudhary Rs, Jain Sp, Sidduqui Fa. B-Sitosterol: Isolation From Muntingia Calabura Linn Bark Extract, Structural Elucidation And Molecular Docking Studies As Potential Inhibitor Of SARS-CoV-2 Mpro (COVID-19). Asian J Pharm Clin Res. 2020;204–9. doi: 10.22159/ajpcr.2020.v13i5.37909.
6. Alhabardi SA, Almutairi JA, Al-Hamoud GA, Zakaraya ZZ, Hani U, Asiri ZAA, et al. Musa Paradisiaca derived intrinsically heteroatom doped carbon dots as antioxidant and controlled drug release behavior. PLoS One. 2025;1–19. doi: 10.1371/journal.pone.0329116.
7. Pham DT, Nguyen DXT, Nguyen NY, Nguyen TTL, Nguyen TQC, Tu AVT, et al. Development of pH-responsive Eudragit S100-functionalized silk fibroin nanoparticles as a prospective drug delivery system. PLoS One. 2024;19(5 May). doi: 10.1371/journal.pone.0303177.
8. Patil VP, Khulb P. Isolation and Identification of Bioactive Chlorogenic Acid from Ethanol Fraction of Cordia subcordata: HPLC, HPTLC, FTIR, and LC-MS Analysis. Int J Pharm Qual Assur. 2024;15(03):1144–50. doi: 10.25258/ijpqa.15.3.07.
9. Vanitha A, Kalimuthu K, Chinnadurai V, Nisha KMJ. Phytochemical screening, FTIR and GCMS analysis of aqueous extract of Caralluma bicolor – An endangered plant. Asian J Pharm Pharmacol. 2019;5(6):1122–30. doi: 10.31024/ajpp.2019.5.6.7.
10. Huang Y, Liu Y, Tan H, Cheng Y, Tao K, Gu D, et al. Assessing essential oil composition in Cinnamomum cassia leaves from different regions of China using GC-MS and FTIR spectroscopy. Czech J Food Sci. 2024;42(3):141–52. doi: 10.17221/197/2023-CJFS.
11. Dezani AB, Pereira TM, Caffaro AM, Reis JM, Serra CH dos R. Equilibrium solubility versus intrinsic dissolution: Characterization of lamivudine, stavudine and zidovudine for BCS classification. Brazilian J Pharm Sci. 2013;49(4):853–63. doi: 10.1590/S1984-82502013000400026.

12. Romdhani A, Martínez F, Chiappetta DA, Peña Á, Jouyban A. Equilibrium Solubility of Acetaminophen in Ternary Mixtures as a Tool for Design of Concentrated Parenteral Medications. J Solution Chem. 2024;53(3):506–23. doi: 10.1007/s10953-023-01347-3.
13. Ramadoss K, Meerasa SS, Satyapal AKS, Vijayakumar A, Venugopal V. Quantitative analysis of favipiravir in bulk and pharmaceutical dosage forms using UV visible spectrophotometer. J Med Pharm Allied Sci. 2023;12(2):5680–3. doi: 10.55522/jmpas.v12i2.4410.
14. Tayeng D, Das S, Das S, Chetia D. UV Spectrophotometric Method Development And Validation For The Combined Plant Extract Traditionally Used In Arunachal Pradesh To Treat Malaria. J Neonatal Surg. 2025;14(30S):975–83. doi: 10.63682/jns.v14i30S.7533.
15. Sawant MP, Deokar GS. Solubility Profiling and UV-Spectrophotometric Determination of Bioactive Peptides from Ragi. Int J Drug Deliv Technol. 2025;15(3):1265–71. doi: 10.25258/ijddt.15.3.47.
16. N V, SK AP, Yadala PC, M S. UV spectrophotometric method for the estimation of pure nicotine. J Innov Appl Pharm Sci. 2025;37–45. doi: 10.37022/jiaps.v10i3.766.
17. Fernández-Pérez A, Marbán G. Visible Light Spectroscopic Analysis of Methylene Blue in Water. J Appl Spectrosc. 2022;88(6):1284–90. doi: 10.1021/acsomega.0c03830.
18. Azadeh M, Gorovits B, Kamerud J, MacMannis S, Safavi A, Sailstad J, et al. Calibration Curves in Quantitative Ligand Binding Assays: Recommendations and Best Practices for Preparation, Design, and Editing of Calibration Curves. AAPS J. 2018;20(1). doi: 10.1208/s12248-017-0159-4.
19. Kumatia EK, Ofosu-Koranteng F, Appiah AA, Barimah KB. Standardization and Quality Control of the Herbal Medicine Mist Nibima, Employed to Treat Malaria and COVID-19, Using Physicochemical and Organoleptic Parameters and Quantification of Chemical Markers via UHPLC-MS/MS. Int J Anal Chem. 2021;2021. doi: 10.1155/2021/6390481.
20. Adebowale ARA, Sanni LO. Effects of solid content and temperature on viscosity of tapioca meal. J Food Sci Technol. 2013;50(3):573–8. doi: 10.1007/s13197-011-0363-7.
21. Ajith K, Pillai AS, Muthu Vijayan Enoch I V., Sharifpur M, Solomon AB, Meyer JP. Effect of the non-electrically conductive spindle on the viscosity measurements of nanofluids subjected to the magnetic field. Colloids Surfaces A Physicochem Eng Asp. 2021;628. doi: 10.1016/j.colsurfa.2021.127252.
22. Zhu W, Long J, Shi M. Release Kinetics Model Fitting of Drugs with Different Structures from Viscose Fabric. Materials (Basel). 2023;16(8). doi: 10.3390/ma16083282.
23. Askarizadeh M, Esfandiari N, Honarvar B, Sajadian SA, Azdarpour A. Kinetic Modeling to Explain the Release of Medicine from Drug Delivery Systems. ChemBioEng Rev. 2023;10(6):1006–49. doi: 10.1002/cben.202300027.
24. Baishya H. Application of Mathematical Models in Drug Release Kinetics of Carbidopa and Levodopa ER Tablets. J Dev Drugs. 2017;06(02). doi: 10.4172/2329-6631.1000171.
25. Tembhare E, Gupta KR, Umekar MJ. An Approach to Drug Stability Studies and Shelf-life Determination. Arch Curr Res Int. 2019;1–20. doi: 10.9734/acri/2019/v19i130147.
26. McKinney E, Deshpande A, Verrilli B, Li C, Sorel D, Kim E, et al. Evaluation of Room Temperature and Accelerated Stability Data For Fitusiran, an Investigational Rnai Therapeutic Targeting Antithrombin for Treatment of Hemophilia and Rare Bleeding Disorders. Haemophilia. 2017;23(S2):59[P051].